24th IMEKO TC4 International Symposium
22nd International Workshop on ADC and DAC Modelling and Testing
IMEKO TC-4 2020
Palermo, Italy, September 14-16, 2020

Distance Calibration of Large PCB Induction-Coil Arrays in Active Mode

Melvin Liebsch[1,2], Olaf Dunkel[1], Andrea Del Carme Fontanet Valls[1], Stephan Russenschuck[1], Stefan Kurz[2]

[1] *European Organization for Nuclear Research, CERN, Geneva, Switzerland*
Melvin.Liebsch@cern.ch, Olaf.Dunkel@cern.ch,
Andrea.Del.Carme.Fontanet.Valls@cern.ch,
Stephan.Russenschuck@cern.ch
[2] *Centre for Computational Engineering, Darmstadt, Germany*
kurz@gsc.tu-darmstadt.de

***Abstract* – Rotating- and translating coil systems for magnetic measurement of particle accelerator magnets rely on induction-coil arrays often built in printed circuit board technology. For the accurate calculation of field gradients from induced voltages, the distances between the coils need to be calibrated. In this paper we present a calibration approach, based on the operation of the PCB in active mode, i.e., exciting the coils with a small current. The resulting flux density distribution is scanned with a uni-axial Hall probe, translated by the stages of a coordinate-measuring machine (CMM). The proposed calibration approach does not rely on field absolutes. Geometric coil distances are computed only from zero crossings of the measured signal. In this way, a low field sensor calibration can be avoided and systematic errors are reduced.**

I. INTRODUCTION

Induction coils built in printed circuit board (PCB) technology are state-of-the-art in magnetic measurements of particle-accelerator magnets. Benefits of this technology result from automated coil fabrication as well as from a higher flexibly in shape design, compared to induction coils made from wires that are wound on a coil support mandrel. The PCB coils are mounted on cylindrical shafts and rotated in the magnet bore to induce voltages by Faraday's law. Integrating the voltage signal in time yields the flux linked with the coil area. Thus, knowing the total surface spanned by the coil windings, one can deduce the average magnetic field intercepted by the sensor. An effective coil area calibration is usually achieved in a homogeneous reference magnet, which itself is calibrated with a nuclear magnetic resonance (NMR) sensor [1].

The sensitivity factor of a radial coil, with respect to a quadrupolar field harmonic $B_2(r_0)$, evaluated at radius r_0, is given by: $S_2^{\text{rad}} = \frac{A}{r_0}(r_2 + r_1)$, where r_2 and r_1 are the outer and inner coil radii and A is the coil surface [2]. Therefore the coil's outer and inner radii must also be calibrated. Fig. 1 shows the cross section of a bad realisation of a PCB, where lateral positioning errors of up to 100 µm between the layers appear. State-of-the-art PCB technology allows for better track positioning with a precision in the ∼ 10 µm range, but the manufacturing of induction-coil arrays for magnetic field measurement is still a particular application for PCB design and requires the examination and fault detection after production. This is why accurate distance calibration of PCB coil arrays is crucial to enable magnetic measurement in the 10^{-4} range. In case of the outer coil of the large PCB illustrated in Fig. 2, $r_2 + r_1 = 334$ mm. In this case, the error estimation based on S_2^{rad} yields a maximum tolerable error of 30 µm, to keep the relative error in B_2 below 10^{-4}. Imperfections of track distances in PCB fabrication can

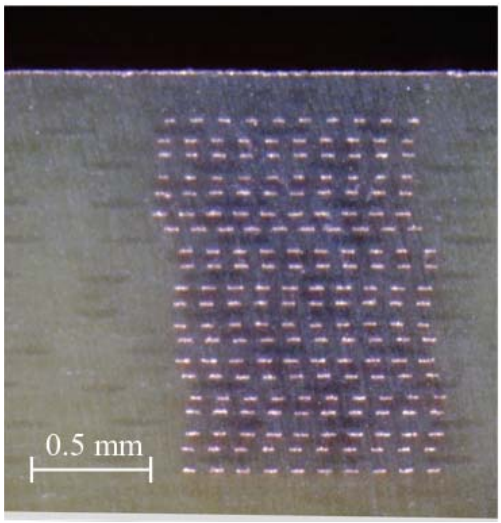

Fig. 1. Cross section of a PCB. The picture shows a "bad" realisation of a multilayer PCB.

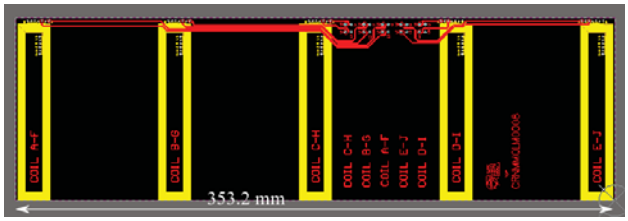

Fig. 2. Layout of an induction-coil array on a large printed-circuit board. The designed distance between the PCB is 83.5 *mm.*

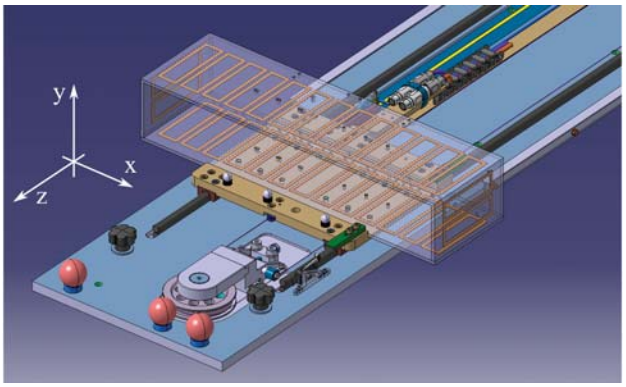

Fig. 3. Design of a stacked translating coil scanner.

be calibrated by rotations in a reference quadrupole, providing a well known field gradient. Local geometry variations are undetectable, however, since the induced voltages are proportional to the entire field integral. Moreover this approach requires a reference magnet, large enough to accommodate the PCB array. Recent demands for large quadrupole-compensated coil arrays have exceeded the capabilities of the available reference quadrupoles (see Fig. 2, [3]). As an alternative, automated optical inspection allows for distance measurement by scanning over the PCB surface optically or by X-ray. However, these methods are rapidly limited in terms of machine size and the fact, that only the visible surface of the PCB can be observed. Often, their utilisation is comparably expensive.

In addition to rotating coil systems, PCB coil arrays are used for local field measurement in translating coil scanners. Fig. 3 illustrates a stacked translating coil scanner, comprising four coil arrays to measure along a box-shaped domain boundary. Since these systems are designed for measurements in large aperture magnets, calibrating the stacking of individual coil arrays would again require large quadrupole magnets, providing a well known gradient. For this reason we propose a novel approach based on the operation of the induction coils in active mode, exciting them with a small current. In order to have a good spatial resolution, we make use of a Hall sensor, translated by a coordinate-measuring

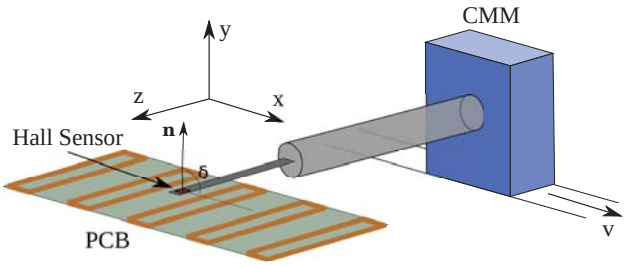

Fig. 4. Sketch of the measurement setup. A Hall sensor is translated by a CMM laterally. The coils in the PCB are powered by a small current. The lateral position x is measured by the linear encoder of the CMM. The Hall voltage is acquired as a signal $U(x)$.

machine (CMM) and scan the generated flux density over the active PCB. A sketch of the measurement setup is shown in Fig. 4.

Throughout this paper we focus on the feasibility and design of the experiment. We test the approach using the PCB coil shown in Fig. 2. Each coil is composed of twelve tracks on twelve layers, leading to an effective coil area of ~ 0.2 m^2 per coil.

II. MEASUREMENT SETUP

To avoid overheating of the PCB, the root mean squared (RMS) excitation current density must not exceed $J_{\mathrm{RMS}} = 1\mathrm{A/mm}^2$. For the track cross section of the PCB in Fig. 2 this yields a maximum excitation current of $I_{\mathrm{DC}} = 5\,\mathrm{mA}$, when powered in direct current (DC) mode. In Fig. 6 we plot the simulated magnetic field, generated with $I = 5\,\mathrm{mA}$, evaluated laterally, at a vertical position of $y = 0.75\,\mathrm{mm}$ above the PCB surface. In this configuration, the absolute magnetic flux density is below 60 µT. It is possible to increase the field by a pulsed excitation with a maximum current I_{max} of:

$$\left(\frac{I_{\mathrm{max}}}{I_{\mathrm{RMS}}}\right)^2 = \frac{T}{T_{\mathrm{p}}}. \tag{1}$$

T_{p} is the pulse duration and T is the waveform period. Increasing the maximum current by a factor of two, one must increase the ratio T/T_{p} by four. Thus a compromise between maximum signal and overall measurement duration has to be found. Fig. 5 sketches the excitation current in pulsed mode. At each lateral position, the PCB is excited with a positive and negative current pulse. This is done for offset cancellation and is explained in more detail in section iii.. The acquisition is synchronised to average the Hall voltage over $T_{\mathrm{aper}} = 50$ ms at the flat top of a current pulse. To assign budget for transient effects at the beginning of each pulse, the T_{aper} interval is delayed by 30 ms. For the measurements presented in section iii., we have chosen $I_{\mathrm{max}} = 25$ mA, $T_{\mathrm{p}} = 100$ ms, yielding $T = 2.5$ s. A Keysight 3458A, 8.5

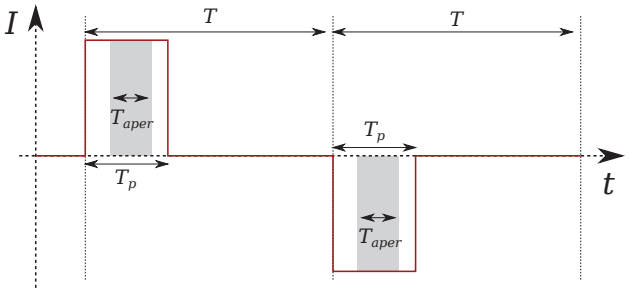

Fig. 5. Excitation current pulses at each lateral position. Subtracting the two Hall voltages acquired over the positive and negative pulse allows to cancel-out temperature dependent offset voltages.

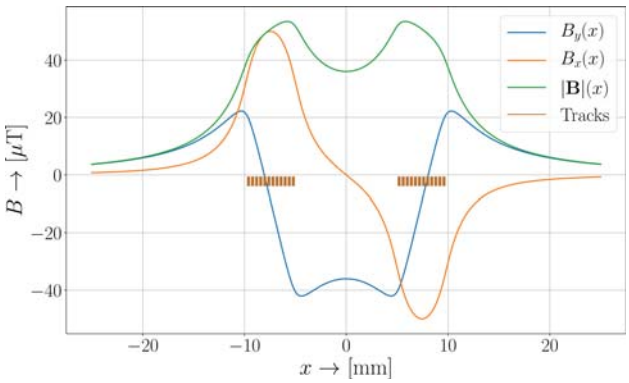

Fig. 6. Simulated flux density over the active PCB. Here $I = 5$ mA. The field is evaluated in 0.75 mm vertical distance over the PCB.

digit digital multimeter is used for the acquisition [4]. We make use of the resting time $T - T_p$ after each second pulse to move the sensor to the next lateral position. In this way, the CMM works in static, single axis positioning mode, unfolding a positioning precision of 2 µm. To estimate the expected signal and to assign a budget for systematic errors, magnetic field simulations are performed. The field scales linearly with $I_{\max}$, comparing to Fig. 6 we thus expect a maximum $|B| \approx 300\,\mu$T, when pulsing the PCB with $I_{\max} = 25$ mA.

A Hall probe, suitable for measurements in this field range is the AS-VTP from Projekt Elektronik [5]. This sensor has an effective area of 0.02 mm^2, a sensitivity of 5000 V/T (with maximum analogue amplification) and a lowest possible measurement range of ±0.2 mT. The sensor characteristics are summarised in Table 1. Dependent on the sensor orientation δ (see Fig. 4), the Hall voltage is proportional to a linear combination of horizontal ($\delta = 0$) and vertical ($\delta = \pi/2$) magnetic flux density, B_x and B_y. Aligning the sensor towards B_y allows us to bring the active area closest to the PCB. For this reason we set $\delta \approx \pi/2$. As illustrated in Fig. 7, any misalignment in δ will introduce an error proportional to B_x,

	AS-VTP
Min. measurement range	±0.2 mT
Transfer function	5000 V/T
Linearity error	$< 0.5\% + 10\,\mu$T
Active area	0.02 mm^2
Typ. peak-peak noise (0-10 Hz)	2 µT
Zero drift	±2µT/K

Table 1. The AS-VTP is tailored to low field measurements and has an active area of 0.02 mm^2. The CMM stages are equipped with an AS-VTP to sample the field generated by the pulsed PCB.

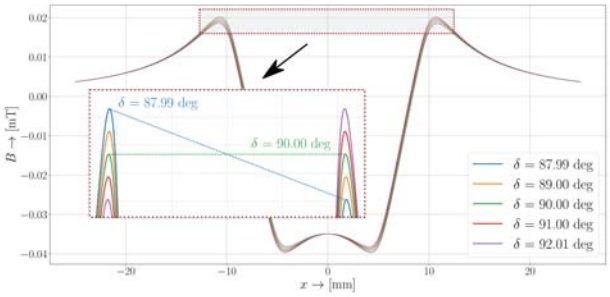

Fig. 7. Effect of misalignment with respect to the lateral flux density distribution $B_y(x)$.

which breaks the signal symmetry. Such misalignment can thus be detected by the difference between the left and right maximum of $B_y(x)$. Since NMR sensors cannot provide a reference measurement in case of low magnetic fields, the accurate calibration of Hall probes under such circumstances is challenging. To avoid errors due to false sensor calibration, we propose an approach that is independent of field absolutes. Based on the acquired Hall voltage, we compute the lateral coil centres x_{ctr}, from left and right zero crossings, denoted by x_{l} and x_{r}. Having determined x_{ctr} for different coils of the array, the computation of coil distances is straight forward. In Fig. 7 we show how misalignment by means of δ breaks signal symmetry and affects the positions x_{l} and x_{r}. However, since x_{ctr} shifts equally for all the coils of the array, coil distances are preserved.

III. ZERO CROSSING DETECTION

Neglecting effects of higher order, we can express the Hall voltage as:

$$U_{\pm}(x) = s\,\mathbf{n}(\delta) \cdot \mathbf{B}(x) + U_0(x, T). \tag{2}$$

s is the sensors linearized field response, $\mathbf{n}(\delta) = (\cos(\delta), \sin(\delta), 0)^T$ is a unit vector pointing normal to the active area of the Hall sensor (see Fig. 4) and $U_0(x, T)$

	x_l	x_r
mean	-7.461 mm	9.027 mm
std	3.439 µm	3.389 µm

Table 2. Repeatability of the zero detection over a single coil. Mean and standard deviation are computed from 8 measurements.

is an offset voltage, dependent on position x and temperature T. Measuring small magnetic fields, a large fraction of $U_0(x,T)$ is attributed to the Earth magnetic and ambient fields due to currents and magnetic material in the proximity of the measurement setup. Thus $U_0(x,T)$ is generally not constant over x. An additional part of $U_0(x,T)$ is coming from the sensors zero-field offset voltage, which generally drifts in T. It is possible to calibrate $U_0(T)$ and then measure T during the acquisition to estimate U_0 at measurement position. However we can simplify things by measuring the Hall voltage generated from a positive and negative excitation current pulse, as illustrated in Fig. 5. Since inverting I_max changes the sign of $\mathbf{B}$, $U_0(x,T)$ vanishes in the difference:

$$U_c(x) = \frac{1}{2}(U_+(x) - U_-(x)) = s\mathbf{n}(\delta)\cdot\mathbf{B}(x), \qquad (3)$$

given that U_0 is equal for U_+ and U_-. Since temperature changes are slow in time, and positive and negative current pulses are taken consecutively, the temperature difference between U_+ and U_- is expected to be neglectable. Since $B_y(x)$ and thus $U_c(x)$ changes its sign twice (see Fig. 6), the coil centre can be computed from $x_\mathrm{ctr} = 0.5(x_\mathrm{l} + x_\mathrm{r})$, where x_l and x_r are left and right zero crossings. Fig. 8 illustrates the mean and 3σ standard deviation of the measured Hall voltage, when pulsing the PCB with a positive and negative current of $|I_\mathrm{max}| = 25$ mA, according to Fig. 5. Mean and standard deviation are computed from 10 runs. The signals settle to $U_0(x,T)$ increasing the distance to the PCB. The temperature close to the Hall element is measured with a Pt100. This temperature is illustrated for one of the 8 runs, in the bottom plot of Fig. 8. It changes by 0.5 K when scanning over the PCB. However, since positive and negative current pulses are taken immediately one after another, the temperature difference between two pulses is neglectable. We now investigate the zero crossings of $U_c(x)$ to determine the lateral positions x_r and x_l. In order to decrease the spatial resolution, we linearly interpolate $U_c(x)$ between the measurement positions in the neighbourhood of the zeros. Fig. 9 shows $U_c(x)$ as well as the left and right interpolation intervals. In table 2 we summarise mean and standard deviations of x_r and x_l.

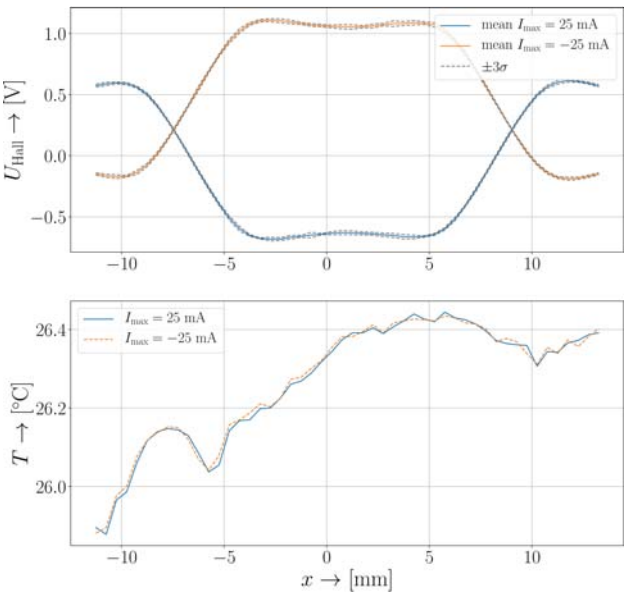

Fig. 8. Measured Hall voltage and temperature over a single coil on the PCB. Top: the signal inverts, when exiting the PCB with a positive or negative current. Mean and standard deviation are computed from 10 repetitions. Bottom: Temperature measured with a Pt100, close to the Hall element. Whereas the temperature changes by 0.5 K, variations between positive (blue) and negative (orange) pulse are neglectable. The probe was moving from $x < 0$ to $x > 0$. The increase in temperature can be explained by the absorption of heat, radiated from the active PCB.

IV. DISTANCE CALIBRATION

The zero crossing detection is now applied to to all the five coils on the PCB. To investigate the repeatability in coil distance calibration, we perform 10 runs at the same longitudinal position. Fig. 10 illustrates U_+ and U_- for one run over coils A to E. The resulting radial positions, as well as standard deviations are summarised in table 3. The designed radial distance between the coils of the measured PCB is $R = 83.5$ mm. We now change the longitudinal position between the runs. Fig. 11 illustrates x_r and x_l over the length of the PCB. In this way, local differences to the design can be investigated (see Fig. 12). To estimate the reproducibility of the calibration procedure, we fully disassemble and reassemble

Coil	R des. [mm]	R meas. [mm]	σ [µm]
A	167	166.992	3.532
B	83.5	83.493	4.168
D	83.5	83.497	2.398
E	167	166.995	4.395

Table 3. Designed (des.) and measured (meas.) radial position of coil A to E, assuming C is centred at $R = 0$.

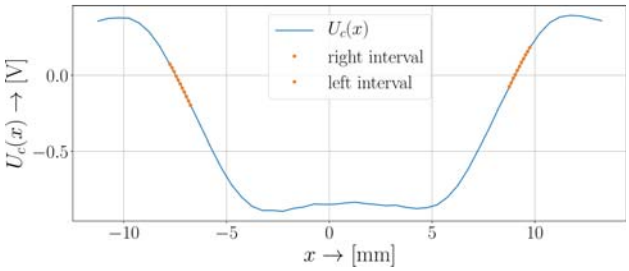

Fig. 9. Offset corrected Hall voltage $U_c(x)$ and zero crossing intervals. To interpolate between measurements (here $\Delta z = 0.1\,\mathrm{mm}$), we fit $U_c(x)$ by lines in the neighbourhoods of the zero crossings (orange).

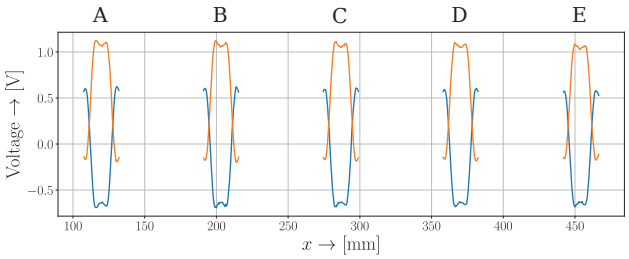

Fig. 10. Hall voltage acquired over coils A to E, exciting the PCB with positive (blue) and negative (orange) current pulses.

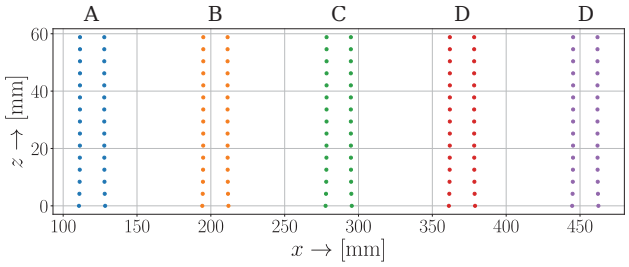

Fig. 11. Left and right zero crossings for all the five coils measured over z.

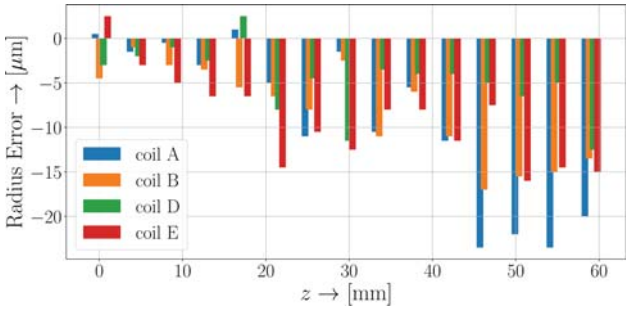

Fig. 12. Differences between designed and measured coil radii over the length of the PCB.

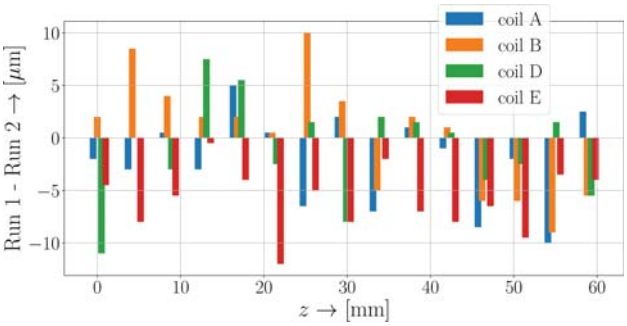

Fig. 13. Differences in coil radii between two calibrations of the same PCB. In between the measurements, the setup was fully dissembled and reassembled.

the measurement setup and repeat the measurements over z. Fig. 13 shows the differences between the two runs over the longitudinal position. The maximum difference is 12 µm.

V. CONCLUSION

We have presented a novel approach for the distance calibration of large PCB coil arrays used in rotating and translating coil scanners. The coil is powered by a pulsed current in the mA range. A Hall sensor, mounted on the stages of a coordinate measurement machine is shifted laterally over the pulsed PCB. Movement and acquisition are synchronised to obtain voltage samples on the flat top of the excitation current pulse. The calibration only relies on the signal zero crossings and is thus independent of field absolutes and sensor calibration. Moreover, switching between positive and negative excitation currents cancels out the influence of ambient fields and temperature dependent zero field offset voltages. In this way, coil distances can be calibrated with a precision of ~ 20 µm, which is sufficient for large PCB coil arrays, such as the radial coil (Fig. 2) designed for [3].

REFERENCES

[1] Reymond C., "Magnetic Resonance Techniques", CERN 98-05, 219-231 (1998).

[2] Russenschuck S., "Field Computation in Accelerator Magnets", John Wiley & Sons, Ltd, 2011.

[3] Cho E. et al., "Preliminary Test Results of the First of Series Multiplet for the Super-FRS at FAIR", IEEE Transactions on Applied Superconductivity, March 2020.

[4] Keysight 3458A Multimeter, Keysight Technologies, Edition 7, January 09, 2020.

[5] Data Sheet AS-Active Probes VTP, Projekt Elektronik Mess- und Regelungstechnik GmbH, page 1, Version 0.2, 28.02.2020.